ACTA IMEKO
ISSN: 2221-870X
March 2026, Volume 15, Number 1, 1 - 7

Improving a linear-quadratic regulator controller by genetic algorithm on a Quanser gyroscope

Hoai-Thuong Luong[1], Minh-Thanh Le[1], Thanh-Tung Pham[1], Chi-Ngon Nguyen[2]

[1] *Vinh Long University of Technology Education, Vinh Long, VietNam*
[2] *Can Tho University, Can Tho, VietNam*

ABSTRACT
In this paper, we present the experimental evaluation of an optimal control solution for the Quanser gyroscope system. To address the challenge of manually tuning the $\boldsymbol{Q}$ and $\boldsymbol{R}$ weighting matrices of the traditional Linear–Quadratic Regulator (LQR) controllers, which performs poorly when system parameters vary, we developed an optimal controller based on a Genetic Algorithm. This method automatically searches for optimal Q and R values based on the Integral of Absolute Error (IAE) criterion, ensuring precise trajectory tracking and fast response. Experimental results demonstrate that the proposed optimal controller exhibits superior performance, with a settling time of 1.98 s, zero overshoot, and a steady-state error of only 0.21 degrees. The most significant contribution of this study, however, is the rigorous experimental implementation and validation of the actual Quanser hardware. Data from the hardware demonstrates the controller's superior, stable operation, enhanced accuracy, and robust dynamic response compared to standard LQR in a real-world environment. These results affirm the potential of the developed method, even when the system is subjected to noise, delays, and nonlinearities. This paper highlights the crucial role of hardware validation in translating theoretical advancements into reliable and effective practical control solutions.

Section: RESEARCH PAPER

Keywords: gyroscope; genetic algorithm; linear-quadratic regulator; experimental validation; Quanser

Citation: H.-T. Luong, M.-T. Le, T.-T. Pham, C.-N. Nguyen, Improving a linear-quadratic regulator controller by genetic algorithm on a Quanser gyroscope, Acta IMEKO, vol. 15 (2026) no. 1, pp. 1-7. DOI: 10.21014/actaimeko.v15i1.2163

Section Editor: Francesco Lamonaca, University of Calabria, Italy

Received August 1, 20256; **In final form** February 26, 20266; **Published** March 20266

Corresponding author: Chi-Ngon Nguyen, e-mail: ncngon@ctu.edu.vn

1. INTRODUCTION

Optimizing control performance is a core area of research, particularly for systems possessing complex dynamics [1]. The gyroscope, characterized by its stability and ability to maintain orientation, has become an essential component in numerous applications, ranging from aerospace and maritime navigation to robotics [2], [3]. Despite its critical role, the inherent nonlinearity and complex dynamics of this system pose a significant challenge to achieving optimal control performance [3]. The Linear–Quadratic Regulator (LQR) is a well-established optimal control method; however, manually tuning its Q and R weighting matrices is a formidable task, especially when system parameters vary, thereby affecting performance [1]. To address this limitation, numerous studies have integrated intelligent optimization algorithms into the controller design problem [4], [5], [6]. In a similar vein, this study introduces a GA-LQR controller, which integrates the Genetic Algorithm (GA) to automate the optimization of the LQR. The controller is designed based on the Integral of Absolute Error (IAE) criterion to significantly enhance the system's trajectory tracking capability and dynamic response.

Although simulation plays a crucial role in the initial design and testing phases, offering a safe and cost-effective means of exploration, it cannot fully replicate complex real-world factors, such as sensor noise, signal delays, nonlinear friction, or unmodeled uncertainties [7]. Consequently, experimental validation on physical hardware becomes an indispensable and paramount requirement to confirm the feasibility and robustness of any control strategy [8]. This process provides irrefutable empirical evidence and can reveal system behaviours not predicted by theoretical models.

As a continuation of previous work on the design and simulation of the GA-LQR controller, the central contribution of this paper is the experimental evaluation of the GA-LQR effectiveness on a real-world Quanser gyroscope platform [9], [10]. The experiments are conducted under identical, rigorous conditions, benchmarking the performance of the GA-LQR against Quanser's standard LQR controller [9]. The objective is

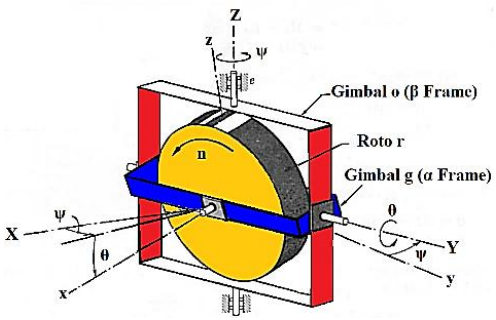

Figure 1. General configuration and coordinates of the gyroscope.

to quantify and demonstrate that the application of the Genetic Algorithm can substantially improve the performance of the LQR controller in a physical environment [8], [11]. This research will also provide an in-depth analysis of the findings and challenges encountered when transitioning from simulation results to the physical system. The remainder of this paper is structured as follows: Section 1 provides the introduction, Section 2 details the methodology, Section 3 presents the simulation and experimental validation, and Section 4 offers the conclusions.

2. METHODOLOGY

2.1. Modelling of the gyroscope

The gyroscope is a classical subject of study in the fields of dynamics and control theory. Figure 1 illustrates the physical model utilized for the analyses. This model represents an idealized version of a typical gyroscope, comprising a rotor (r) that spins at a constant angular velocity, denoted by n, relative to the inner gimbal (g). The orientation of the system is described by two angular coordinates, θ and ψ, within a fixed inertial frame of reference [12].

To construct the simulation model, the research team analyzed the gyroscope system depicted in Figure 1, based on the fundamental principles of mechanics and drawing reference from sources [12], [13], [14]. The system is a mechanism with two degrees of freedom (2-DOF), where its state is defined by two angular coordinates, θ and ψ. This system is analyzed using two nested reference frames: Frame α attached to the inner gimbal (g) and Frame β attached to the outer gimbal (o). The vector sum of the angular velocities of these reference frames determines the angular velocity of the rotor (Ω^{r}):

$$\Omega^{\beta} = 1_z\,\dot{\psi}\,, \tag{1}$$

$$\begin{aligned}\Omega^{\alpha} &= \Omega^{\alpha/\beta} + \Omega^{\beta} = 1_y\,\dot{\theta} + 1_z\,\dot{\psi} \\ &= -1_x\,\dot{\psi}\sin\theta + 1_y\,\dot{\theta} + 1_z\,\dot{\psi}\cos\theta\end{aligned} \tag{2}$$

$$\begin{aligned}\Omega^{\mathrm{r}} &= \Omega^{\mathrm{r}/\alpha} + \Omega^{\alpha} = 1_x\,n + 1_y\,\dot{\theta} + 1_z\,\dot{\psi} \\ &= 1_x\big(n - \dot{\psi}\sin\theta\big) + 1_y\,\dot{\theta} + 1_z\,\dot{\psi}\cos\theta.\end{aligned} \tag{3}$$

Here, 1_x, 1_y, and 1_z denote the unit vectors along the x, y, and z axes, respectively, consistent with the notation used in [12]. The system's equations of motion are established from Euler's moment equation, wherein the applied external moment, M_{i}, is equal to the rate of change of the angular momentum, H:

$$-M_i^{\mathrm{r}} = \dot{H}^{\mathrm{r}} = \overset{\alpha}{H}{}^{r} + \Omega^{\alpha} \times H^{\mathrm{r}}, \tag{4}$$

$$-M_i^{\mathrm{g}} = \dot{H}^{\mathrm{g}} = \overset{\alpha}{H}{}^{\mathrm{g}} + \Omega^{\alpha} \times H^{\mathrm{g}}, \tag{5}$$

$$-M_i^{0} = \dot{H}^{0} = \overset{\beta}{H}{}^{0} + \Omega^{\beta} \times H^{0}. \tag{6}$$

Applying this principle, the moment balance equations are written for each component. For the rotor and inner gimbal assembly (g + r), considering the moment balance about the y-axis:

$$(\Sigma M^{*})_y = \big(M_i^{\mathrm{r}} + M_i^{\mathrm{g}}\big)_y + M_{\mathrm{b}} = 0\,. \tag{7}$$

For the entire system (g + r + o), considering the moment balance about the z-axis:

$$(\Sigma M^{*})_z = \big(M_i^{\mathrm{r}} + M_i^{\mathrm{g}} + M_i^{\mathrm{o}}\big)_z + M_{\mathrm{c}} = 0\,. \tag{8}$$

If we analyse the gyroscope's role as a gyrocompass, equation (8) is expanded as follows:

$$\big(M_i^{\mathrm{r}} + M_i^{\mathrm{g}}\big)_z \cos\theta - \big(M_i^{\mathrm{r}} + M_i^{\mathrm{g}}\big)_z \sin\theta + (M_i^{o})_z + M_{\mathrm{c}} = 0\,. \tag{9}$$

Substituting the Euler equations (4), (5), and (6) into the moment balance equations (7), (8), and (9), the general equations of motion are obtained:

$$H^{\mathrm{r}} = 1_x J_x^{\mathrm{r}}\big(n - \dot{\psi}\sin\theta\big) + 1_y J_y^{\mathrm{r}}\,\dot{\theta} + 1_z J_z^{\mathrm{r}}\,\dot{\psi}\cos\theta\,, \tag{10}$$

$$H^{\mathrm{g}} = -1_x J_x^{\mathrm{g}}\,\dot{\psi}\sin\theta + 1_y J_y^{\mathrm{g}}\,\dot{\theta} + 1_z J_z^{\mathrm{g}}\,\dot{\psi}\cos\theta\,, \tag{11}$$

$$H^{\mathrm{o}} = 1_z J_z^{\mathrm{o}}\,\dot{\psi}\,. \tag{12}$$

Where the system's moment components and products of inertia are defined in:

$$h \triangleq J_x^{\mathrm{r}}\,n\,, J_x \triangleq +J_x^{\mathrm{g}}, J_y \triangleq J_y^{\mathrm{r}} + J_y^{\mathrm{g}},\; J_z \triangleq J_z^{\mathrm{r}} + J_z^{\mathrm{g}}. \tag{13}$$

Substituting the inertia expressions (13) into the general equations (10), (11), and (12), the complete nonlinear dynamic equations of motion are obtained:

$$\begin{aligned}&-\big(M_i^{\mathrm{r}} + M_i^{\mathrm{g}}\big)_y \\ &\qquad = J_y\,\ddot{\theta} + h\,\dot{\psi}\cos\theta + (J_z - J_x)\,\dot{\psi}^2\sin\theta\cos\theta\,,\end{aligned} \tag{14}$$

$$\begin{aligned}&-\big(M_i^{\mathrm{r}} + M_i^{\mathrm{g}}\big)_z\cos\theta \\ &\qquad = J_z\big(\ddot{\psi}\cos^2\theta - \dot{\psi}\,\dot{\theta}\sin\theta\cos\theta\big) - h\,\dot{\theta}\cos\theta \\ &\qquad + \big(J_x - J_y\big)\,\dot{\psi}\,\dot{\theta}\sin\theta\cos\theta\,,\end{aligned} \tag{15}$$

$$\begin{aligned}&-\big(M_i^{\mathrm{r}} + M_i^{\mathrm{g}}\big)_z\sin\theta \\ &\qquad = -J_z\big(\ddot{\psi}\sin^2\theta + \dot{\psi}\,\dot{\theta}\cos\theta\sin\theta\big) \\ &\qquad + \big(J_z - J_y\big)\,\dot{\psi}\,\dot{\theta}\cos\theta\sin\theta\,.\end{aligned} \tag{16}$$

Combining the terms and substituting equations (14), (15), and (16) into (7) and (9) yields:

$$J_y\,\ddot{\theta} + h\,\dot{\psi}\cos\theta + (J_z - J_x)\,\dot{\psi}^2\sin\theta\cos\theta = M_{\mathrm{b}}, \tag{17}$$

$$\begin{aligned}&\big(J_z^{o} + J_z\cos^2\theta + J_x\sin^2\theta\big)\,\ddot{\psi} - h\,\dot{\theta}\cos\theta \\ &\qquad + 2\,(J_x - J_z)\,\dot{\psi}\,\dot{\theta}\sin\theta\cos\theta = M_{\mathrm{c}}\,.\end{aligned} \tag{18}$$

To analyse the small oscillations around the equilibrium position, the system of equations (17) and (18) is linearized. This process is based on the following assumptions: the rotation angles ψ and θ are very small, and the rotor's spin rate, n, is

tremendous and constant. The result of this linearization is the system of equations of motion for a two-axis gyroscope under small oscillation conditions:

$$\begin{cases} J_y\,\ddot{\theta} + h\,\dot{\psi} = M_{\mathrm{b}}\,, \\ J_z\,\ddot{\psi} - h\,\dot{\theta} = M_{\mathrm{c}}\,. \end{cases} \tag{19}$$

Where M_{b} and M_{c} are the external moments acting on the inner and outer gimbal axes, respectively. The Quanser gyroscope model is a special case of this general model, simplified for controller design by assuming that only a control torque, τ_{y}, is applied to one axis, while no external force acts on the other [9], [10]:

$$\begin{cases} J_y\,\ddot{\theta} + h\,\dot{\psi} = \tau_y \\ J_z\,\ddot{\psi} - h\,\dot{\theta} = 0 \end{cases}. \tag{20}$$

The parameters for the Quanser gyroscope system, detailed in the manufacturer's technical documentation, are presented in Table 1 [9], [10].

The system of equations (20) describes the dynamics of the system. As the next step, for modern control analysis and design, this model will be converted into its state-space representation**:**

The state vector of the system is explicitly defined as $\boldsymbol{x} = \left[\theta, \psi, \dot{\theta}, \dot{\psi}\right]^{\mathrm{T}}$ where θ and ψ represent the pitch and yaw angles, respectively, and $\dot{\theta}$, ψ represent their corresponding angular velocities.

$$\dot{x} = \boldsymbol{A}\,x + \boldsymbol{B}\,u \tag{21}$$

$$y = \boldsymbol{C}\,x + \boldsymbol{D}\,u\,. \tag{22}$$

The system matrices are determined according to the Quanser technical documentation [9], [10]. For the 3 DOF Gyroscope systems, these matrices are defined as: $\boldsymbol{A}$ = [0, 0, -109.9557, 0; 0, 0, 1, 0; 19.7230, 0, 0, 0; 0, 1, 0, 0], $\boldsymbol{B}$ = [250; 0; 0; 0], $\boldsymbol{C}$ = [0, 1, 0, 0], and $\boldsymbol{D}$ = [0].

2.2. LQR controller design

The LQR is an optimal control algorithm used to determine the optimal pole placement for a system. The LQR design process requires defining a performance index and solving the Algebraic Riccati Equation (ARE) to obtain the optimal control gain. Specifically, the objective of LQR is to design a state-feedback controller, K, that minimizes a performance index, J. In this method, the feedback gain matrix $\boldsymbol{K}$ is designed to minimize a cost function, thereby achieving a trade-off between control effort, state significance, and response speed, which ensures a stable system [1], [7]. The designer selects appropriate $\boldsymbol{Q}$ and $\boldsymbol{R}$ weighting matrices to determine the ideal gain matrix $\boldsymbol{K}$, a task often performed using a software such as MATLAB. The structure of the LQR controller is illustrated in Figure 2, where: ψ_{ref} is the reference signal, and ψ_{act} is the actual system output. With the LQR control law defined by:

$$\boldsymbol{u(t)} = -\boldsymbol{K} \cdot \boldsymbol{x(t)}\,. \tag{23}$$

Table 1. Quanser gyroscope parameters.

Symbol	Value	Description
J_y	0.0039 kg · m²	Inner Gimbal Moment of Inertia
J_z	0.0223 kg · m²	Outer Gimbal Moment of Inertia
h	0.44 kg · m² / s	Rotor Angular Momentum

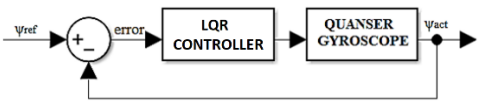

Figure 2. LQR controller block diagram.

The weighting matrices are selected according to the Quanser technical documentation [9], [10], where the control penalty weight is set to $\boldsymbol{R}$ = [5] and the state weighting matrix $\boldsymbol{Q}$ is $\boldsymbol{Q}$ = diag([2, 16, 0.01, 0.0001]).

Determining the optimal gain matrix, $\boldsymbol{K}$, is contingent upon solving the Continuous-time Algebraic Riccati Equation. The objective is to find the unique, symmetric, and positive definite solution, $\boldsymbol{P}$, for the equation [15]:

$$\boldsymbol{A}^{\mathrm{T}}\,\boldsymbol{P} + \boldsymbol{P}\,\boldsymbol{A} - \boldsymbol{P}\,\boldsymbol{B}\,\boldsymbol{R}^{-1}\,\boldsymbol{B}^{\mathrm{T}}\,\boldsymbol{P} + \boldsymbol{Q} = 0\,. \tag{24}$$

Once the solution $\boldsymbol{P}$ of equation (24) is determined, the state-feedback gain matrix $\boldsymbol{K}$ is calculated directly from the following expression:

$$\boldsymbol{K} = \boldsymbol{R}^{-1}\,\boldsymbol{B}^{\mathrm{T}}\,\boldsymbol{P}\,. \tag{25}$$

Applying the method above to the system under study, with the predefined weighting matrices $\boldsymbol{Q}$ and $\boldsymbol{R}$, equations (24) and (25) are solved numerically using the LQR function in the MATLAB environment. The resulting feedback gain matrix, $\boldsymbol{K}$, is obtained as follows: $\boldsymbol{K}$ = [0.65, 1.79, 0.12, 0.0045].

2.3. Design of the optimal GA-LQR controller

The GA is applied to determine the optimal parameters for the weighting matrices, $\boldsymbol{Q}$ and $\boldsymbol{R}$, of the standard Quanser LQR controller. The GA automatically searches for the values of Q and R within a vast search space, independent of any empirical methods. The task of the GA is to select the optimal set of parameters for the LQR controller's weighting matrices, $\boldsymbol{Q}$ and $\boldsymbol{R}$, such that the Integral of Absolute Error (IAE) cost function, as shown in equation (26) and illustrated in the diagram in Figure 3, is minimized.

The optimization problem to determine the optimal Q_{opt} and R_{opt} values was addressed using a GA implemented in MATLAB. This paper employs the GA as a practical tool, with its underlying principles detailed in references [5], [11], [16], [17], [18]. The chromosome structure encodes the diagonal elements of the weighting matrix $\boldsymbol{Q}$ and the scalar R as real-valued genes. To ensure the asymptotic stability of the LQR controller, the search space for these parameters was strictly bounded to positive values (lower bound > 0), thereby guaranteeing that the resulting $\boldsymbol{Q}$ and $\boldsymbol{R}$ matrices remain positive definite. The operational sequence of the Genetic Algorithm is visually summarized in Figure 4.

The GA, as defined by (26) and (27), will perform the optimization based on the cost function referenced in [19], [20], [21], [22]. The optimization process was conducted offline using the simulation model to ensure the safety of the physical

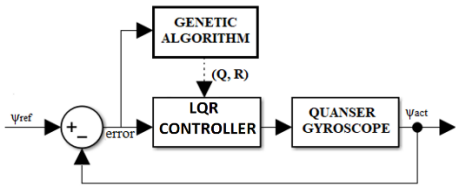

Figure 3. GA-LQR controller block diagram.

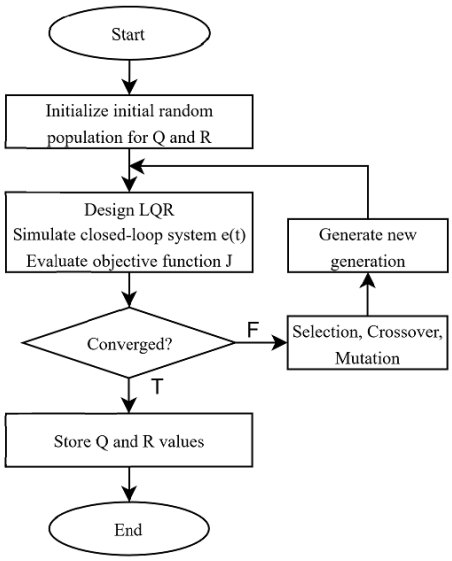

Figure 4. Flowchart of the Genetic Algorithm for finding Q and R parameters.

mechanism and computational efficiency before hardware implementation. The Integral of Absolute Error (IAE) was selected as the cost function because it offers a balanced trade-off between transient response speed and steady-state precision, avoiding the excessive overshoot often associated with ISE or the slow settling time typical of ITAE.

$$IAE: J = \int_0^{\infty} |e(t)| \, \mathrm{d}t \,, \tag{26}$$

Where $e(t) = \psi_{\mathrm{ref}}(t) - \psi_{\mathrm{act}}(t)$. The GA is applied to find the optimal values of Q_{opt} and R_{opt} for the LQR controller that minimizes the function J. Therefore, the objective function for the GA is:

$$Fitness = \min\{J\} \,. \tag{27}$$

To constrain the search space of the GA, we hypothesize that the optimal values, Q_{opt} and R_{opt}, lie within a specific range surrounding the values recommended by Quanser [9], [10]. Determining these bounds is necessary to limit the search space, as searching within an unbounded domain would be computationally expensive and inefficient.

$$\begin{cases} 0.01 \times Q_{\mathrm{quanser}} \leq Q_{\mathrm{opt}} \leq 100 \times Q_{\mathrm{quanser}} \\ 0.01 \times R_{\mathrm{quanser}} \leq R_{\mathrm{opt}} \leq 100 \times R_{\mathrm{quanser}} \end{cases} . \tag{28}$$

These bounds are established based on the initial values referenced from Quanser, with the lower bound set to 0.01 times and the upper bound to 100 times the corresponding initial value.

2.4. Experimental setup

Figure 5 illustrates the connection diagram of the experimental setup. The system comprises a Quanser gyroscope connected to a host computer via a Q8-USB interface card and an AMPAQ-L4 amplifier. The control signal from the computer is processed by the interface card, amplified, and subsequently supplied to the motor. Conversely, the feedback signal from the optical encoders is transmitted back to the computer through the Q8 card, thereby forming a closed-loop control system. The entire algorithm is designed using QUARC within the MATLAB/Simulink environment. It is executed directly on the Q8-USB card with a sampling period of 1 ms. This sampling frequency (1 kHz) was selected based on the hardware

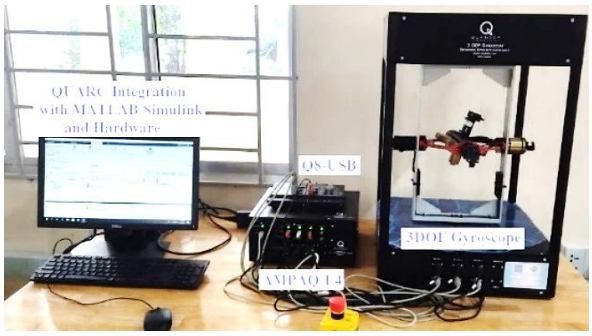

Figure 5. Connection diagram of the experimental setup.

specifications of the Quanser Q8-USB interface [9], [10] to ensure real-time stability and to minimize discretization delays, which is critical for the fast dynamics of the gyroscope system. This process is visually demonstrated in the experimental video [23].

The initial setup phase of the experimental procedure, shown in Figure 6, aims to identify the equilibrium point and calibrate the system to ensure the accuracy of data acquisition.

3. SIMULATION AND EXPERIMENTAL RESULTS

3.1. Simulation results

Upon convergence of the Genetic Algorithm, the optimal weighting matrices were identified as: $\boldsymbol{Q_{\mathrm{opt}}}$ = diag([0.01, 772.17, 0.37, 0.02]) and R_{opt} = 1.18.

These optimized values were subsequently used for both the simulation and the experimental validation on the physical hardware.

To evaluate the controller's trajectory tracking performance, two types of reference signals were utilized. The first signal is a square wave with an amplitude of 20 and a frequency of 0.1 Hz, as defined by equation (29):

$$\psi_{\mathrm{ref}}(t) = 20 \cdot \mathrm{square}(0.2\,\pi\,t) \,. \tag{29}$$

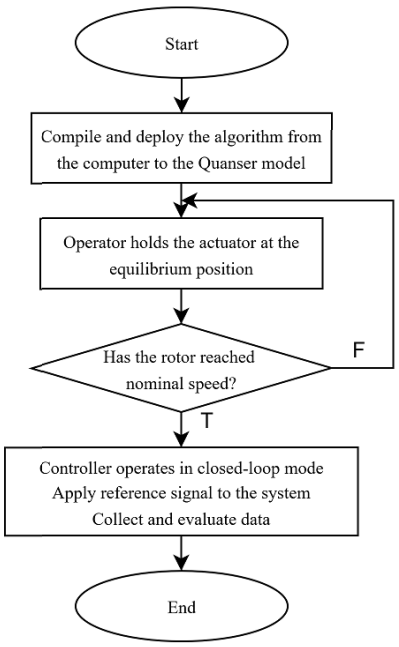

Figure 6. Experimental procedure on the physical model.

As shown in Figure 7, The responses of both the LQR and GA-LQR controllers show good trajectory tracking capability with minor errors. However, the GA-LQR demonstrates markedly superior performance during the transient phases (at 5 s, 10 s, 15 s, and 25 s), with a significantly faster and more precise response. This improvement proves that the optimization process using the Genetic Algorithm has enhanced the system's dynamics, thereby reducing the settling time.

Figure 8 illustrates that the GA-LQR control signal exhibits a larger magnitude and shorter duration of action compared to the standard LQR control signal. This demonstrates the superior speed and precision in trajectory tracking of the GA-LQR, which is a direct result of the optimization process using the GA. The second signal is a sine wave with an amplitude of 20 and a frequency of 0.1 Hz, as defined by equation (30):

$$\psi_{\text{ref}}(t) = 20 \cdot \sin(0.2\,\pi\,t)\,. \tag{30}$$

For the sinusoidal reference trajectory, both the LQR and GA-LQR controllers tracked the path very well. However, the GA-LQR still demonstrated more precise tracking and less phase lag, further affirming its superior performance. The tracking performance for the sinusoidal reference is illustrated in Figure 9. The LQR controller optimized by the GA yields a superior response compared to the standard Quanser LQR controller, with a settling time of 1.72 seconds and no overshoot, as detailed in Table 2.

3.2. Experimental results

The primary objective of this study is to evaluate and compare the experimental performance of the proposed GA-LQR controller with that of the standard LQR controller, implemented directly on the Quanser gyroscope system. The trajectory tracking performance of the two controllers was verified using the reference signals (29) and (30). Through this process, the controllers' performance was validated in a physical environment subject to noise, nonlinearities, and other uncertainties.

The experimental results indicate that both the LQR and GA-LQR controllers ensure trajectory tracking capability. However, the GA-LQR controller demonstrates superior performance, particularly with a faster response and more precise tracking during the transient phases, which helps to reduce the system's settling time. The experimental results for the square wave trajectory are presented in Figure 10. Compared to the simulation results, the actual response exhibits a certain amount of noise and minor oscillations. This phenomenon is an inevitable consequence of physical factors, including friction, motor inertia, and the inherent nonlinear characteristics of the mechanical system.

Figure 11 illustrates that the GA-LQR control signal in the experimental setup still has a higher initial magnitude compared to the LQR. This directly contributes to its faster and more effective response in the real-world system.

For the sinusoidal reference trajectory (30), although both controllers effectively tracked the path, the GA-LQR controller demonstrated markedly superior performance, with a

Table 2. Comparison of system quality criteria.

Performance Criteria (ψ)	LQR	GA-LQR
Overshoot (%)	0	0
Settling Time (s)	2.0	1.72
Steady-State Error (deg)	0.92	0.11

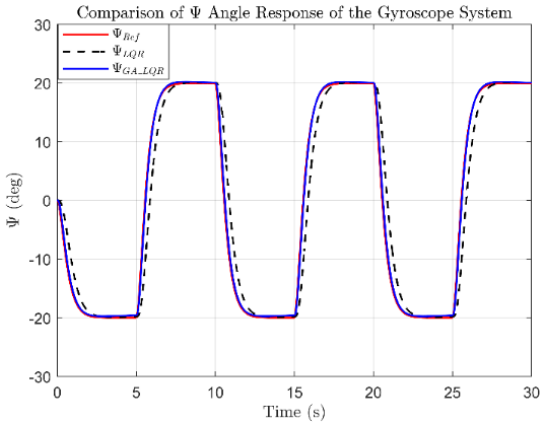

Figure 7. Simulated response of angle ψ for LQR and GA-LQR.

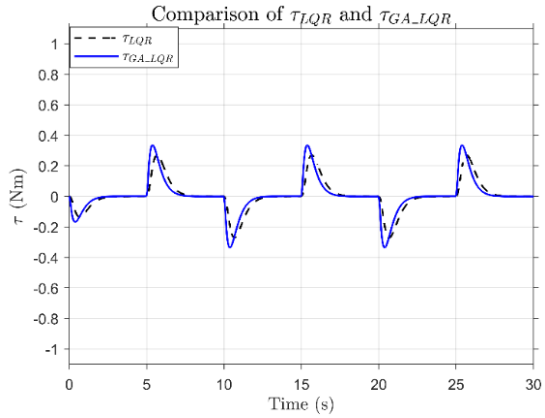

Figure 8. Simulated control response of LQR and GA-LQR.

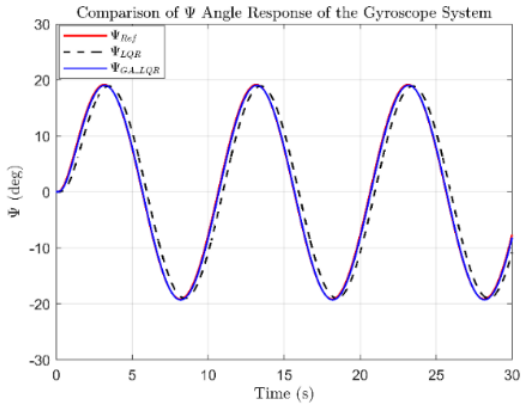

Figure 9. Simulated response of angle ψ for LQR and GA-LQR.

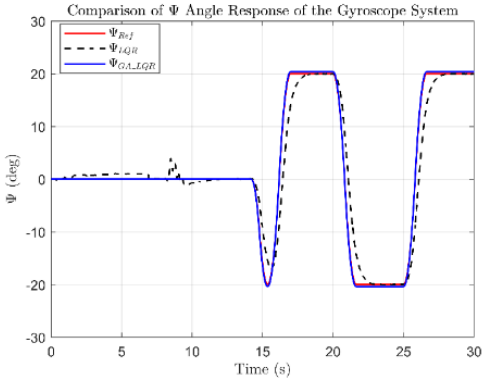

Figure 10. Experimental response of angle ψ for LQR and GA-LQR.

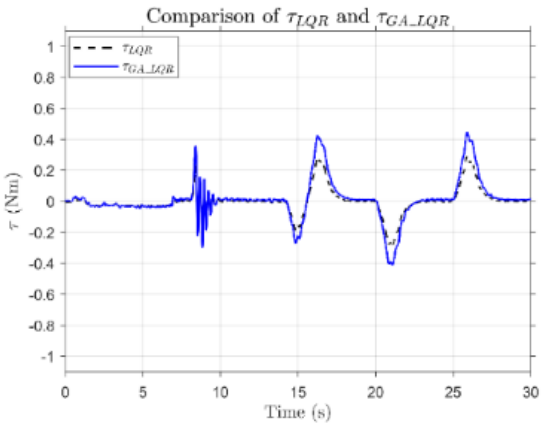

Figure 11. Experimental control response of LQR and GA-LQR.

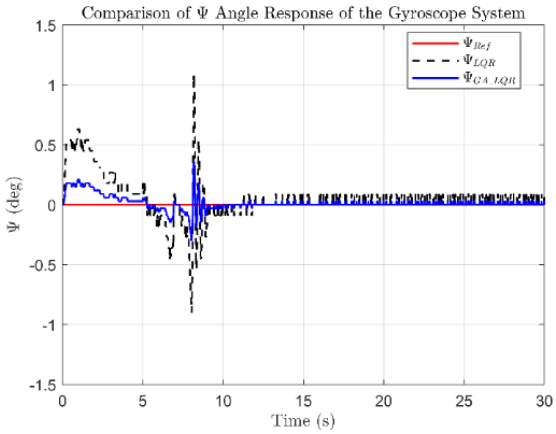

Figure 13. Experimental control response of LQR and GA-LQR.

significantly reduced amplitude error and phase lag. Figure 12 demonstrates the experimental performance of the system when following a sinusoidal reference. This result affirms the high performance and stability of the GA-LQR algorithm, particularly when tracking continuously varying trajectories in a physical environment subject to noise and nonlinearities.

Figure 13 presents the experimental response of the system with the two different controllers at the equilibrium point. The analysis of the graph can be divided into two distinct phases. Phase before 10 seconds: This is the system's start-up period. As previously discussed, during this interval, the gyroscope's rotor is accelerating to reach its nominal speed. Consequently, the responses of both controllers exhibit large and unstable oscillations, which do not accurately reflect the actual performance of the algorithms. Phase after 10 seconds: This is the steady-state operational phase, serving as the basis for performance evaluation. Observation shows that the response of the standard LQR controller still displays slight oscillations before settling at the zero value. In contrast, the GA-LQR controller demonstrates clear superiority. Its response stabilizes almost instantaneously at zero, with negligible deviation and no overshoot. The system's performance parameters are quantitatively detailed in Table 3 for comparison and benchmarking against the simulation results.

The quantitative analysis from Table 2 and Table 3 reveals that the GA-LQR controller exhibits superior performance compared to the standard LQR controller. Specifically, in simulation, the GA-LQR achieves a settling time of 1.72 s and a steady-state error of 0.11 degrees. During experimental validation of the physical system, these performance metrics remained excellent, with a settling time of 1.98 seconds and a steady-state error of 0.21 degrees. An ideal overshoot of 0 % was maintained in both environments.

Although the experimental performance shows a slight degradation compared to the simulation, this discrepancy is attributed to physical factors that are not fully modelled, such as friction, noise, and hardware imperfections. The controller's effective performance in the real-world environment demonstrates its high robustness and its ability to compensate for these deviations.

It is worth noting that at a reference amplitude of 20 degrees (≈ 0.35 rad), the system operates near the limit of the small-angle approximation ($\sin\theta \approx \theta$) assumed in the linear model. Despite the emergence of nonlinear effects in this regime, the experimental results demonstrate that the GA-LQR controller maintains high tracking accuracy and stability. This confirms the robustness of the optimized parameters, which effectively compensate for the unmodeled nonlinear dynamics and physical uncertainties, such as friction and sensor noise.

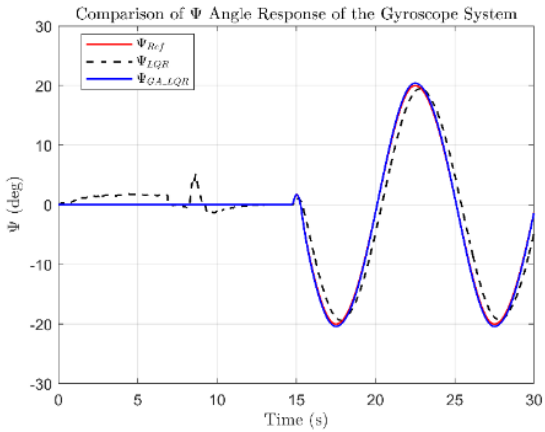

Figure 12. Experimental response of angle ψ for LQR and GA-LQR.

4. CONCLUSION

This paper presents the design and validation of a GA-LQR controller on a physical Quanser hardware platform. The method of offline optimization of LQR parameters using a Genetic Algorithm proved advantageous, as it does not require a detailed mathematical model of the system.

The research demonstrated that the GA-LQR solution significantly improves system performance compared to the standard LQR controller. The experimental results successfully validated the design's effectiveness, demonstrating a rapid, precise, and stable response with high correspondence to the simulation results. The primary contribution of this work is the establishment of a validated framework that bridges the gap between theoretical GA optimization and practical hardware implementation. We demonstrate that an offline simulation-based optimization, when properly constrained, can yield a robust controller capable of handling real-world uncertainties,

Table 3. Comparison of system quality criteria from experimental results.

Performance Criteria (ψ)	LQR	GA-LQR
Overshoot (%)	0	0
Settling Time (s)	2.26	1.98
Steady-State Error (deg)	1.05	0.21

without the complexity of online tuning or nonlinear control structures.

Future research directions may focus on enhancing the controller's robustness and developing real-time adaptive control solutions.

AUTHORS' CONTRIBUTION

Mr. Luong Hoai Thuong, first author, is a PhD student under the supervision of Prof. Dr. Chi-Ngon Nguyen (last and corresponding author), who has prepared the manuscript. Dr. Le Minh Thanh, 2nd author, has contributed to model simulation. Prof. Dr. Pham Thanh Tung, 3rd author, has contributed to writing correction. Prof. Dr. Chi-Ngon Nguyen is the Chief of the research group, who has supervised this study and finalized this paper.

ACKNOWLEDGEMENT

We are deeply grateful to the Intelligent Control Laboratory at Vinh Long University of Technology Education for their essential support. The successful validation of our algorithm was made possible by the laboratory's provision of an excellent working environment and access to the Quanser experimental system, which was funded by the ADB project.

5. REFERENCES

[1] N. S. Nise, Control Systems Engineering, 8th ed. Hoboken, NJ: John Wiley & Sons, Inc., 2020.

[2] J. Fang, J. Qin, Advances in Atomic Gyroscopes: A View from Inertial Navigation Applications, Sensors, vol. 12 (2012) no. 5, pp. 6331-6346. DOI: 10.3390/s120506331

[3] W. A. Gill, I. Howard, I. Mazhar, K. K. Mckee, A Review of MEMS Vibrating Gyroscopes and Their Reliability Issues in Harsh Environments, Sensors, vol. 22 (2022) no. 19, p. 7405. DOI: 10.3390/s22197405

[4] T. Ahmmed, I. Akhter, S. M. R. Karim, F. A. S. Ahamed, Genetic Algorithm Based PID Parameter Optimization, American Journal of Intelligent Systems, vol. 10 (2020) no. 1, pp. 21-32. DOI: 10.5923/j.ajis.20201001.02

[5] C. N. Ngon, PID controller optimization using genetic algorithm, Can Tho University Journal of Science, no. 9, pp. 241-248, 2008. Online [Accessed 23 February 2026] [in Vietnamese] https://sj.ctu.edu.vn/ql/docgia/download/baibao-5029/q_KHNN_241_248.pdf

[6] R. Sharma, K. P. S. Rana, V. Kumar, Statistical analysis of GA based PID controller optimization for robotic manipulator, Proc. of the Int. Conf. on Issues and Challenges in Intelligent Computing Techniques (ICICT), Ghaziabad, India, 7-8 February2014, pp. 1-6. DOI: 10.1109/ICICICT.2014.6781368

[7] D. Shetty and R. A. Kolk, Mechatronics System Design. Boston, MA: Cengage Learning, 2017.

[8] S. M. Ahmad, S. Fareed, Attitude modelling and real-time robust control of a 3-DoF quadcopter UAV test bench, The Aeronautical Journal, vol. 128 (2024) no. 1324, pp. 1047-1070. DOI: 10.1017/aer.2024.11

[9] Quanser Inc., 3 DOF Gyroscope Laboratory Guide, 2013. Online [Accessed 23 February 2026] https://drive.google.com/file/d/1MCUhjErsnKFtTdauCuCIOHFFwBTo1kg9/view

[10] Quanser Inc., 3-DOF Gyroscope, 2025. Online [Accessed 23 February 2026] https://www.quanser.com/products/3-dof-gyroscope/

[11] M. T. Le, N. C. Ngon, L. H. Thuong, T. T. Pham, C. T. Phan, Performance Evaluation Of Fuzzy-PID And GA-PID Controllers On A 3-DOF Delta Robot Tracking Control, Proc. of the 2022 Int. Conf. on Control, Robotics and Informatics (ICCRI), Danang, Vietnam, 2-4 April 2022, pp. 1-10. DOI: 10.1109/ICCRI55461.2022.00008

[12] R. H. Cannon, Jr., Dynamics of Physical Systems. Mineola, NY: Dover Publications, 2012.

[13] T. Sasaki, T. Shimomura, H. Schaub, Robust Attitude Control Using a Double-Gimbal Variable-Speed Control Moment Gyroscope, Journal of Spacecraft and Rockets, vol. 55 (2018) no. 5, pp. 1235-1247. DOI: 10.2514/1.A34120

[14] D. Stevenson, H. Schaub, Nonlinear Control Analysis of a Double-Gimbal Variable-Speed Control Moment Gyroscope, Journal of Guidance, Control, and Dynamics, vol. 35 (2012) no. 3, 2012, pp. 787-793. DOI: 10.2514/1.56104

[15] K. Ogata, Modern Control Engineering, 5th ed. Upper Saddle River, NJ: Prentice Hall, 2010.

[16] MathWorks, Optimization with MATLAB and the Genetic Algorithm and Direct Search Toolbox. Online [Accessed 23 February 2026] https://www.mathworks.com/matlabcentral/fileexchange/6232-optimization-with-matlab-and-the-genetic-algorithm-and-direct-search-toolbox

[17] MathWorks, How can I tune PID controller using Genetic Algorithm? Online [Accessed 23 February 2026] https://www.mathworks.com/matlabcentral/answers/53760-how-can-i-tune-pid-controller-using-genetic-algorithm

[18] M. T. Le, H. T. Luong, T. T. Pham, C. T. Phan, C.-N. Nguyen, Optimization of PID controller by genetic algorithm experiment on delta robot, Measurement, Control, and Automation, vol. 26 (2022) no. 2, pp. 57-65. Online [Accessed 23 February 2026] [in Vietnamese] https://drive.google.com/file/d/1bIoVQs4F2xvN7k7pn5mGoedfrNji8zWe/view?usp=sharing

[19] A. Alouache, Q. Wu, Genetic Algorithms for Trajectory Tracking of Mobile Robot Based on PID Controller, Proc. of the IEEE 14th Int. Conf. on Intelligent Computer Communication and Processing (ICCP), Cluj-Napoca, Romania, 6-8 September2018, pp. 357-362. DOI: 10.1109/ICCP.2018.8516587

[20] E. Flores-Morán, W. Yánez-Pazmiño, J. Barzola-Monteses, Genetic algorithm and fuzzy self-tuning PID for DC motor position controllers, Proc. of the International Carpathian Control Conference (ICCC), Szilvasvarad, Hungary, 28-31 May 2018, pp. 164-169. DOI: 10.1109/CarpathianCC.2018.8399621

[21] D. C. Meena, A. Devanshu, Genetic algorithm tuned PID controller for process control, Proc. of the Int. Conf. on Inventive Systems and Control (ICISC), Coimbatore, India, 19-20 January2017, pp. 1-6. DOI: 10.1109/ICISC.2017.8068639

[22] L. A. Yusuf, N. Magaji, GA-PID controller for position control of inverted pendulum, Proc. of the Int. Conf. on Adaptive Science & Technology (ICAST), Ota, Nigeria, 29-31 October 2014, pp. 1-6. DOI: 10.1109/ICASTECH.2014.7068099

[23] H. T. Lunong, Experimental GA-LQR Control of a Quanser 3-DOF Gyroscope, YouTube, Jul. 10, 2025. Online video [Accessed 23 February 2026] https://www.youtube.com/watch?v=_bg3xonXhXs